Unified Robust Zero-Error Tracking Control of CVCF PWM Converters

Keliang Zhou and Danwei Wang

Abstract—This paper proposes a unified robust zero-error tracking control scheme for constant-voltage-constant-frequency (CVCF) PWM converters to eliminate the tracking error in the presence. Based on the internal model principle, the proposed control scheme plugs a reference signal generator into the stable conventional feedback closed-loop system to accomplish zero error tracking of the dc or ac reference input. The design of the unified zero error tracking controller is systematically developed and the stability analysis of overall control system is discussed. Three examples of the proposed controlled CVCF converters, such as CVCF PWM inverter, boost-type PWM rectifier, and dc–dc PWM buck converter are studied to testify the validity of the proposed approach. Simulation and experimental results demonstrate satisfactory performance of the proposed unified robust zero error tracking controller even under parameter uncertainties and load disturbances.

Index Terms—PWM converter, repitited control.

I. INTRODUCTION

CONSTANT-voltage-constant-frequency (CVCF) PWM converters, such as dc–dc boost and buck converters, dc–ac inverters, and ac–dc rectifiers, are widely employed in various power supplies. A good power supply should have the nominal constant output under disturbances and uncertainties, good dynamic response to disturbances, and remain stable under all operating conditions.

During the past decades, many attempts have been made to develop various control schemes for CVCF PWM converters to meet with the above demands, such as deadbeat control [1]–[4], sliding mode control [5]–[7] and hysteresis control [8], [9]. Whereas, the deadbeat control leads to a sampling interval delay between the reference and the output and is also highly dependent on the accuracy of the parameters; random switching pattern of hysteresis control may cause the difficulty of low-pass filtering and may impose excessive stress on power device under heavy loads; discrete sliding mode control is robust to disturbances, but might degrade performance with a limited sampling rate. Although proportional-integral-derivative (PID) controllers provide robust zero error tracking for dc reference input and repetitive controllers are effective in tracking ac periodic reference inputs [10]–[14], the complete synthesis method and stability analysis of unified zero error tracking (URZET) controllers for CVCF PWM converters are not established.

In this paper, based on the internal model principle [15], a discrete time unified robust zero error tracking controller is proposed for CVCF PWM converters with fixed switching frequency. The design of URZET controller with universal plug-in structure is systematically presented. The stability of overall system is discussed in detail. Based on the presented method, URZET controllers for dc–ac CVCF PWM inverter, ac–dc boost-type PWM rectifier, and dc–dc buck converters are developed to be the application examples. Simulation and experimental results are provided to support the claim.

II. UNIFIED ROBUST ZERO-ERROR TRACKING CONTROLLER

Let's consider a discrete time control system as shown in Fig. 1, where $y_d(z)$ is reference input signal, $y(z)$ is output signal, $d(z)$ is disturbance signal, $e(z)$ is the tracking error signal, $G_s(z)$ is the transfer function of the plant, $G_g(z)$ is the reference signal generator; plug-in controller $G_{gc}(z)$ is the plug-in compensator, and $G_c(z)$ is the original conventional feedback controller, e.g., PD controller. Before the plug-in of controller $G_{gc}(z), G_c(z)$ is chosen so that the following closed-loop transfer function is asymptotically stable

$$H(z) = \frac{G_c(z)G_s(z)}{1 + G_c(z)G_s(z)} = \frac{z^{-d}B(z^{-1})}{A(z^{-1})}$$
$$= \frac{z^{-d}B^+(z^{-1})B^-(z^{-1})}{A(z^{-1})} \tag{1}$$

where d is the known number of pure time step delays; $B^-(z^{-1})$ is the uncancelable portion of $B(z^{-1})$; $B^+(z^{-1})$ is the cancelable portion of $B(z^{-1})$.

The z-transform of the transfer function $G_g(z)$ for step dc signal or periodic ac signal generator can be expressed as

$$G_g(z) = \frac{k_g z^{-N_1}}{1 - z^{-N}} = \frac{k_g z^{N_2}}{z^N - 1} \tag{2}$$

where k_g is the *control gain*; for ac reference inputs, $N = f/f_c = N_1 + N_2$ with f being the reference signal frequency and f_c being the sampling frequency; for dc reference input, $N = N_1 = 1$ and $N_2 = 0$.

Based on the internal model principle [15], the zero error tracking of any reference input in the steady state can be achieved if a generator of the reference input is included in the stable closed-loop system. Therefore, for dc or ac reference inputs, the controller $G_{gc}(z)$ should include a signal generator $G_g(z)$ as follows:

$$G_{gc}(z) = G_g(z)G_f(z) \tag{3}$$
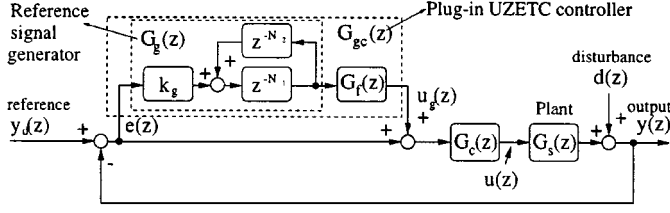
Fig. 1. Plug-in zero error tracking control system.

where G_f is low-pass filter. For dc reference inputs, $G_f(z)$ is usually chosen as follows:

$$G_f(z) = 1 \qquad (4)$$

and for ac reference inputs, $G_f(z)$ is chosen in the following form [16]:

$$G_f(z) = \frac{z^{-n_u} A(z^{-1}) B^-(z)}{B^+(z^{-1})b} \qquad (5)$$

where $N_2 = n_u + d; B^-(z)$ is obtained from $B^-(z^{-1})$ with z^{-1} replaced by $z; b$ is a scalar chosen so that $b \geq [B^-(1)]^2; n_u$ is the order of $B^-(z^{-1})$, and z^{-n_u} makes the filter realizable. $G_f(z)$ (5) is a *Zero Phase Error Tracking Controller* [17].

Obviously, for systems with dc reference inputs, (3) is a discrete time integral controller, and $G_{gc}(z)$ plus $G_c(z)$ is a discrete time PID controller; for systems with ac reference inputs, (3) is a discrete time *repetitive controller*. Repetitive controllers are widely found in industry applications [18]–[20]. Therefore, (3) is the unified approach of integral controllers and repetitive controllers.

From Fig. 1, the transfer functions from $y_d(z)$ and $d(z)$ to $y(z)$ in the overall in the closed-loop control system are, respectively, derived as

$$\frac{y(z)}{y_d(z)} = \frac{(1 + G_g(z)G_f(z))G_c(z)G_s(z)}{1 + (1 + G_g(z)G_f(z))G_c(z)G_s(z)}$$
$$= \frac{(1 - z^{-N} + k_g z^{-N_1} G_f(z))H(z)}{1 - z^{-N}(1 - k_g z^{-N_2} G_f(z)H(z))} \qquad (6)$$

$$\frac{y(z)}{d(z)} = \frac{1}{1 + G_c(z)G_s(z)}(1 - z^{-N})$$
$$\times \frac{1}{1 - z^{-N}(1 - k_g z^{N_2} G_f(z)H(z))}. \qquad (7)$$

From (6) and (7), it can be concluded that the overall closed-loop system is stable if the following two conditions hold: 1) The roots of $1 + G_c(z)G_s(z) = 0$ are inside the unit circle, and 2)

$$\|1 - k_g z^{N_2} G_f(z)H(z)\| < 1, \quad \text{for all } z = e^{j\omega}, \quad 0 < \omega < \frac{\pi}{T}. \qquad (8)$$

However, in practice, there exists model uncertainty for plant. Let the unmodeled dynamics $\Delta(z)$ be represented in the form of a multiplicative modeling error. It is assumed that there exists a constant ϵ such that $\|\Delta(z)\| \leq \epsilon$. The relation between the true system transfer function $H_t(z)$ and the nominal system transfer function $H(z)$ can be written as

$$H_t(z) = H(z)(1 + \Delta(z)) \qquad (9)$$

where all poles of $H_t(z)$ are inside the unit circle.

Then, for PID control systems, (8) leads to a conservative stable range for k_g as follows:

$$0 < k_g < \frac{2}{\max \|H(z)\| + \epsilon}. \qquad (10)$$

In view of (1), (5) and (9), it can be derived that

$$G_f(z)H_t(z) = \frac{z^{-N_2} B^-(z)B^-(z^{-1})}{b} + \Delta(z). \qquad (11)$$

Therefore, for repetitive control systems, (8) yields

$$0 < k_g < \frac{2}{\max \|B^-(z)B^-(z^{-1})/b + \Delta(z)\|} \leq \frac{2}{1 + \epsilon}. \qquad (12)$$

From Fig. 1, the error transfer function for the overall system is

$$G_e(z) = \frac{e(z)}{y_d(z) - d(z)} = \frac{1}{1 + G_c(z)G_s(z)}(1 - z^{-N})$$
$$\times \frac{1}{1 - z^{-N}(1 - k_g z^{N_2} G_f(z)H_t(z))}. \qquad (13)$$

Obviously, if the overall closed-loop system shown in Fig. 1 is asymptotically stable and the angular frequency ω of the reference input $y_d(t)$ and the disturbance $d(t)$ approaches $\omega_m = 2\pi m f, m = 0, 1, 2, \ldots, M$ ($M = N/2$ for even N and $M = (N-1)/2$ for odd N), then $z^{-N} \to 1, \lim_{\omega \to \omega_m} \|G_e(j\omega)\| = 0$, and thus

$$\lim_{\omega \to \omega_m} \|e(j\omega)\| = 0. \qquad (14)$$

Notice that when $y_d(t)$ and $d(t)$ are dc signals, their angular frequency $\omega = 0$. Hence, (14) indicates that, if the frequency of reference input or disturbance is less than half of the sampling frequency, zero steady-state tracking errors for both dc and ac reference inputs are ensured using plug-in controller $G_{gc}(z)$ [12], even in the presence of modeling uncertainty. For CVCF PWM converters, reference inputs are constant dc inputs or CVCF sinusoidal ac inputs. Therefore, the plug-in controller $G_{gc}(z)$ (3) is the unified robust zero error tracking controller for CVCF PWM converters with fixed switching frequency.

It should be pointed out that the repetitive controller can eliminate dc tracking error, too. However, if N is large, it will take too longer regulation time for plug-in repetitive controller to eliminate the dc error. Besides, comparing with integral controller, the size of the memory for the implementation of the repetitive controller is larger. Therefore, for dc reference input, plug-in integral controller is preferred.

To enhance the robustness of the system, a low-pass filter $Q(z, z^{-1})$ can be used in $G_g(z)$ as follows [18]:

$$G_g(z) = \frac{k_g Q(z, z^{-1}) z^{-N_1}}{1 - Q(z, z^{-1}) z^{-N}} \qquad (15)$$

where

$$Q(z, z^{-1}) = \frac{\sum_{i=0}^{m} \alpha_i z^i + \sum_{i=1}^{m} \alpha_i z^{-i}}{2 \sum_{i=1}^{m} \alpha_i + \alpha_0} \qquad (16)$$

where α_i $(i = 0, 1, \ldots, m; m = 0, 1, 2, \ldots)$ are coefficients to be designed.

Notice that $Q(z, z^{-1})$ is a moving average filter that has zero phase shift and bring all open loop poles inside the unit circle
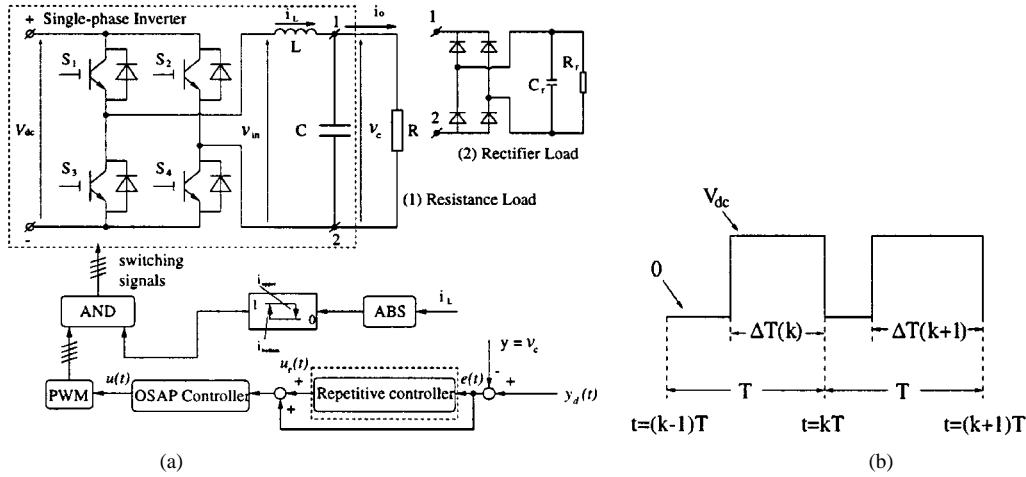
Fig. 2.   Single-phase CVCF PWM inverter and PWM input waveform.

except the one at $+1$. A first order filter $Q(z, z^{-1}) = (z + 2 + z^{-1})/4$ is generally sufficient. On the other hand, high frequency periodic disturbances are not perfectly canceled by this controller. In this case, a trade-off is made between tracking precision and system robustness. And correspondingly, (8) is modified as follows [19]:

$$\|1 - k_g z^{N_2} G_f(z) H_t(z)\| < 1 \leq \left\| \frac{1}{Q(z, z^{-1})} \right\|. \quad (17)$$

The next few sections provide three design examples of URZET controllers for CVCF PWM converters.

III. EXAMPLE 1: SINGLE-PHASE CVCF PWM INVERTER

In the discrete time domain, the dynamics of the CVCF PWM dc-ac converter with resistance load (as shown in Fig. 2(a)) can be described as follows [1]:

$$\begin{bmatrix} v_c(k+1) \\ \dot{v}_c(k+1) \end{bmatrix} = \begin{bmatrix} \varphi_{11} & \varphi_{12} \\ \varphi_{21} & \varphi_{22} \end{bmatrix} \begin{bmatrix} v_c(k) \\ \dot{v}_c(k) \end{bmatrix} \pm \begin{bmatrix} g_1 \\ g_2 \end{bmatrix} \Delta T(k) \quad (18)$$

and its output equation is

$$y(k) = v_c(k) \quad (19)$$

where $\varphi_{11} = 1 - (T^2/2L_nC_n)$; $\varphi_{21} = -(T/L_nC_n) + (T^2/2L_nC_n^2R_n)$; $\varphi_{12} = T - (T^2/2C_nR_n)$; $\varphi_{22} = 1 - (T/C_nR_n) - (T^2/2L_nC_n) + (T^2/2C_n^2R_n^2)$; $g_1 = (v_{\mathrm{dcn}}T/2L_nC_n)$; $g_2 = (v_{\mathrm{dcn}}/L_nC_n)(1 - (T/2C_nR_n))$; v_c is the output voltage; i_o is the output current; v_{dcn} is the nominal dc bus voltage; L_n, C_n, and R_n are the nominal values of the inductor, capacitor and load, respectively; as shown in Fig. 2(b), the control input v_{in} is a PWM voltage pulse of magnitude v_{dc} (or $-v_{\mathrm{dc}}$) with width ΔT in the sampling interval T.

ARMA equation for the system (18), (19) can be derived as follows:

$$y(k+1) = -p_1 y(k) - p_2 y(k-1) + m_1 u(k) + m_2 u(k-1) \quad (20)$$

where $u(k) = \pm\Delta T(k)$; $p_1 = -(\varphi_{11} + \varphi_{22})$, $p_2 = \varphi_{11}\varphi_{22} - \varphi_{21}\varphi_{12}$, $m_1 = g_1$, $m_2 = g_2\varphi_{12} - g_1\varphi_{22}$. The objective of the controller is to force the tracking error between $y(k)$ and its sinusoidal reference $y_d(k)$ with the period of $N*T$ to approach zero asymptotically.

A. Controller Design

One Sampling Ahead Preview (OSAP) controller [1] for the plant (20) is chosen as follows:

$$u(k) = \frac{1}{m_1}[y_d(k) - m_2 u(k-1) + p_1 y(k) + p_2 y(k-1)] \quad (21)$$

then $y(k+1) = y_d(k)$. It yields deadbeat response with transfer function $H(z) = z^{-1}$.

In order to overcome one sampling interval delay of OSAP and the influence of the uncertainties $\Delta L, \Delta C \Delta R$ and Δv_{dc}, for the sinusoidal reference input, a plug-in URZET controller—repetitive controller $G_{gc}(z)$ is proposed as follows:

$$G_{gc}(z) = G_g(z)G_f(z) = \frac{k_g Q(z, z^{-1})z^{-N+1}}{1 - Q(z, z^{-1})z^{-N}} \quad (22)$$

where $G_f(z) = (1/H(z)) = z$; $G_g(z) = (k_g Q(z, z^{-1})z^{-N_1})/(1 - Q(z, z^{-1})z^{-N})$; $N_2 = 0$; $N_1 = N$; $Q(z, z^{-1}) = d_1 z + d_0 + d_1 z^{-1}$ is used to enhance the robustness of the system. If $Q(z, z^{-1}) = 1$, in sampled-data form, the repetitive controller (22) can be expressed as follows:

$$u_g(k) = u_r(k - N) + k_g e(k - N + 1) \quad (23)$$

In fact, (23) is the same as the anticipatory learning control law [21].

B. Robustness Analysis

With the uncertainties and disturbance $\Delta L, \Delta C, \Delta v_{\mathrm{dc}}$ and ΔR, the ARMA equation for the actual plant becomes

$$y(k+1) = -a_1 y(k) - a_2 y(k-1) + b_1 u(k) + b_2 u(k-1) \quad (24)$$

where $a_1 = p_1 + \Delta p_1, a_2 = p_2 + \Delta p_2, b_1 = m_1 + \Delta m_1$ and $b_2 = m_2 + \Delta m_2$ are calculated on the basis of the practical parameters $L = L_n + \Delta L, C = C_n + \Delta C, v_{\mathrm{dc}} = v_{\mathrm{dcn}} + \Delta v_{\mathrm{dc}}$ and $R = R_n + \Delta R$.

When the OSAP controller (21) is applied to the plant (24), the true transfer function $H_t(z)$ becomes (25) shown at the bottom of the next page. According to the stability analysis in Section II, the overall system is stable if: 1) all poles of (25) are inside the unit circle; 2) $\|1 - k_g z H_t(z)\| < 1 \leq \|(1/Q(z, z^{-1}))\|$.

(a)   (b)
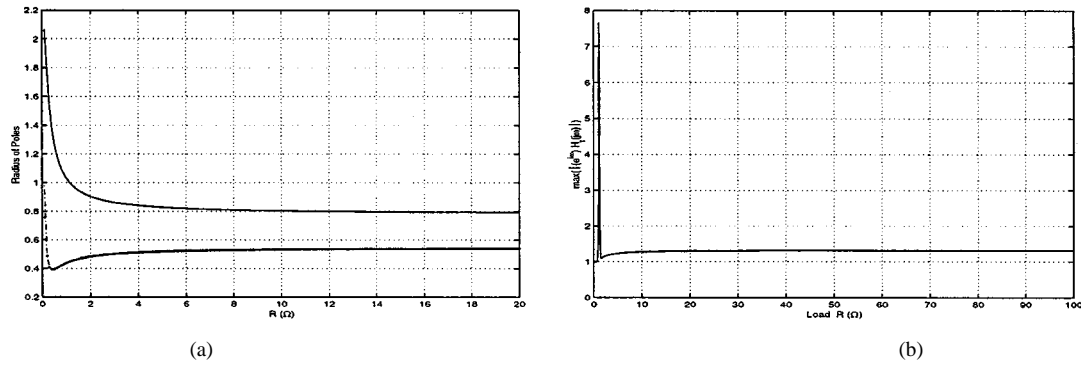
Fig. 3.   Stability Analysis.

(a)   (b)
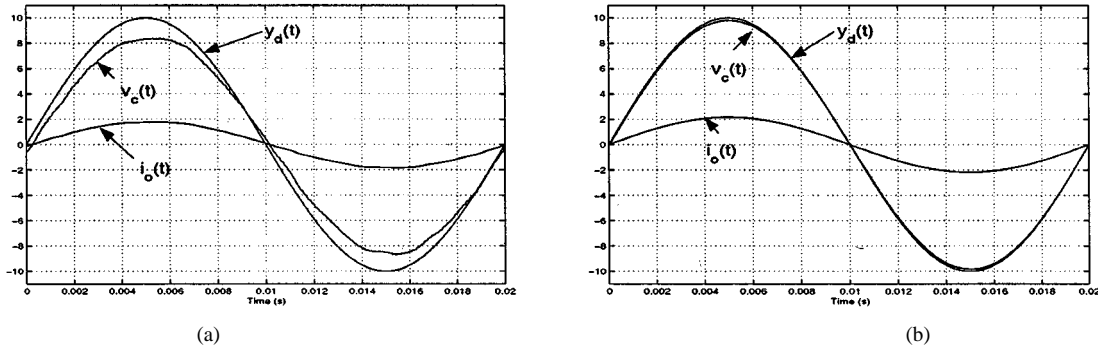
Fig. 4.   Steady-state simulation results with resistance load $R = 4.7\ \Omega$.

C. Simulation and Experiment

Parameter values in the simulations and experiments: $C_n = 800\ \mu\text{F}$; $L_n = 700\ \mu\text{H}$; $R_n = 2\ \Omega$; $v_{\text{dcn}} = 40$ V; $C = 700\ \mu\text{F}$, $L = 600\ \mu\text{H}$; $y_d(t)$ is 50 Hz, 10 V (peak) sinusoidal signal; $v_{\text{dc}} = 20$ V; $f = 50$ Hz; $f_c = (1/T) = 6.25$ kHz; $d_0 = 0.9, d_1 = 0.05; N = f_c/f = 125$.

As shown in Fig. 3(a), with these parameter values and when $R > 1\ \Omega$, all the poles of the closed-loop transfer function $H_t(z)$ in (25) without repetitive controller are located inside the unit circle, the system is stable. And as shown in Fig. 3(b), the maximum gain of $zH_t(z)$ in frequency domain is no more than 8. According to the stability condition $\|1 - k_g z H_t(z)\| < 1$ for repetitive control design, the system with repetitive controller is stable if $k_g \in (0, 0.25)$. We choose $k_g = 0.03$.

Under some transient cases, such as plug-in of rectifier load, overcurrent might occur. Without an internal current regulator, the power switches should be shut down when the transient overcurrent flowing through switches is detected, and then the whole inverter system stops working. In practice, in order to overcome the transient overcurrent, an internal hysteresis current regulator is used. If the peak of inductor currents i_L exceeds a upper threshold value i_{upper}, all switches will be dynamically turned

off; if the peak of i_L drops to be less than a lower threshold value i_{bottom}, the switches will return working immediately. Hence the currents that flow through power switches will be limited by the threshold value i_{upper}. In the simulations and experiments, $i_{\text{upper}} = 10$ A and $i_{\text{bottom}} = 5$ A.

1) Simulation Results: Figs. 4 and 5 show the simulation results of the only OSAP controlled and OSAP plus repetitive controlled CVCF PWM dc/ac converter with resistance load and uncontrolled rectifier load, respectively. With OSAP controller, the peaks of tracking error $e(t)$ between the output voltage and the reference voltage are about 1.8 V in Fig. 4(a) and about 2.3 V in Fig. 5(a), respectively. Figs. 4(b) and 5(b) show that repetitive controller force the output voltage approach reference voltage under different loads and significantly reduced the tracking error, respectively.

Figs. 6 and 7 show the simulation results of OSAP plus repetitive controlled transient responses with/without internal current regulator when a uncontrolled rectifier load ($C_1 = 1.5$ mF, $R_1 = 9.4\ \Omega$) is plugged in. Without an internal current regulator, the output transient current i_o surges to be above 10 A and the peak of inductor currents reaches 14 A; with an internal current regulator, the output transient current i_o drops to 7 A and the peak of inductor currents is restricted to be less than 10 A.

$$H_t(z) = \frac{(b_1 + b_2 z^{-1})}{(z + a_1 + a_2 z^{-1})(m_1 + m_2 z^{-1}) - (p_1 + p_2 z^{-1})(b_1 + b_2 z^{-1})} \tag{25}$$

(a)

(b)
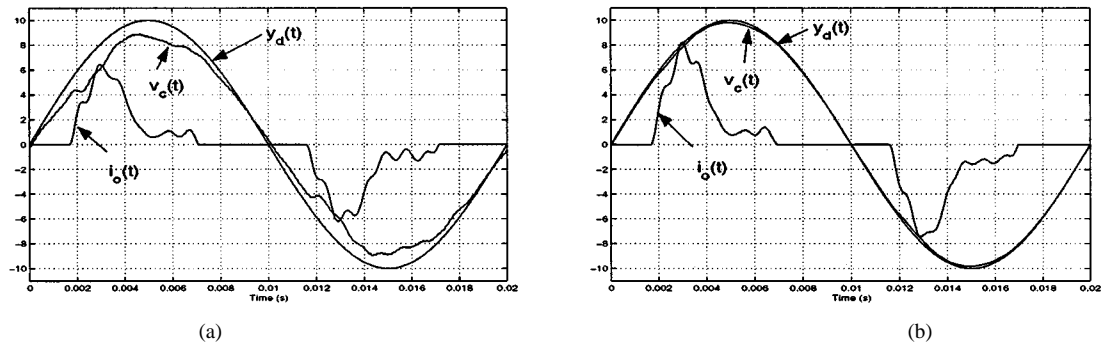
Fig. 5. Steady-state simulation results with rectifier load $R_r = 4.7\ \Omega$, $C_r = 1470\ \mu F$.

(a)

(b)
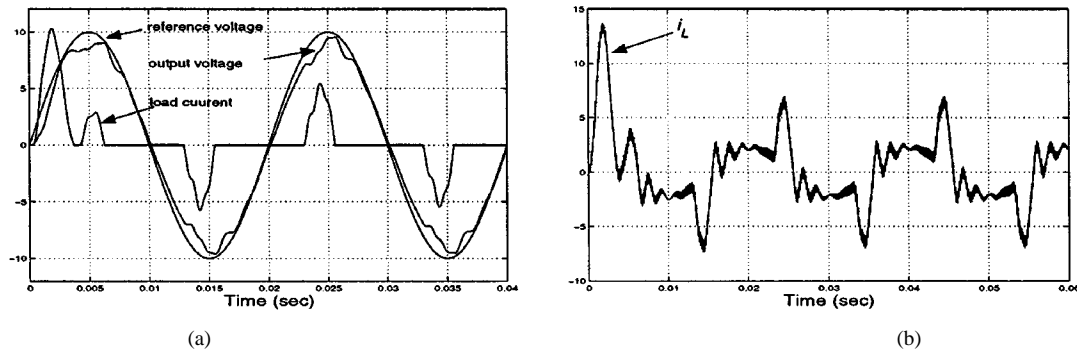
Fig. 6. Simulated transient response without current regulator.

(a)

(b)
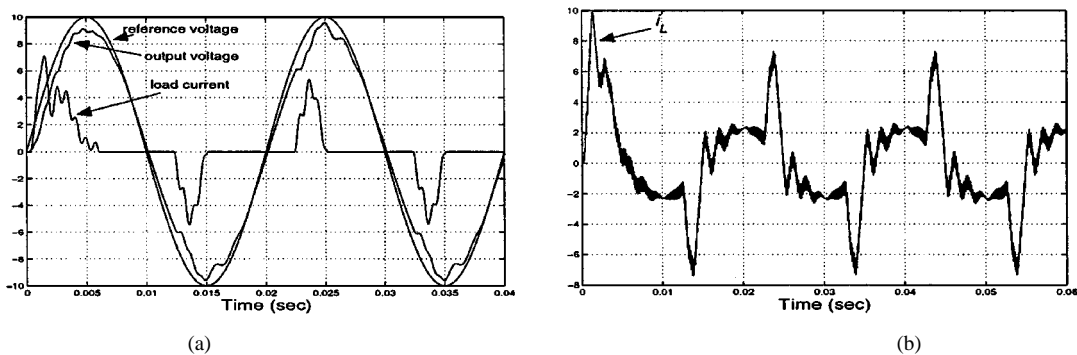
Fig. 7. Simulated transient response with current regulator.

Obviously, the internal current regulator can successfully overcome the transient overcurrent. Therefore, the system is robust to the transient current surge.

2) Experimental Results: Experiment setup, as shown in Fig. 8, has been built for the converter system shown in Fig. 2(a). Facilities include DSPACE (DS1102) DSP development toolkits, H-bridge IGBT switches converter and HP 546002 oscilloscope. Dead time for IGBT power switches is 3 μS. DSP computational delay is about 30 μS.

Fig. 9 shows the experimental results of the only OSAP and OSAP plus repetitive controlled CVCF PWM dc/ac converter under resistance load $(R = 4.7\ \Omega)$. Output voltage is about 8.2 V with OSAP controller in Fig. 9(a), $\text{THD} = 0.6\%$; output voltage approaches 10 V with OSAP plus repetitive controller in Fig. 9(b), $\text{THD} = 0.4\%$. Furthermore, Fig. 9(c) shows the tracking error $e(t)$ is reduced from about 1.8 V to be less than 0.3 V after about 4 seconds when repetitive controller is plugged into the OSAP controlled converter.

Fig. 8. Experiment setup.

Fig. 10 shows the experimental results of the only OSAP and OSAP plus repetitive-controlled CVCF PWM dc/ac converter under uncontrolled rectifier load $(C_r = 1470\ \mu F, R_r = 4.7\ \Omega)$.
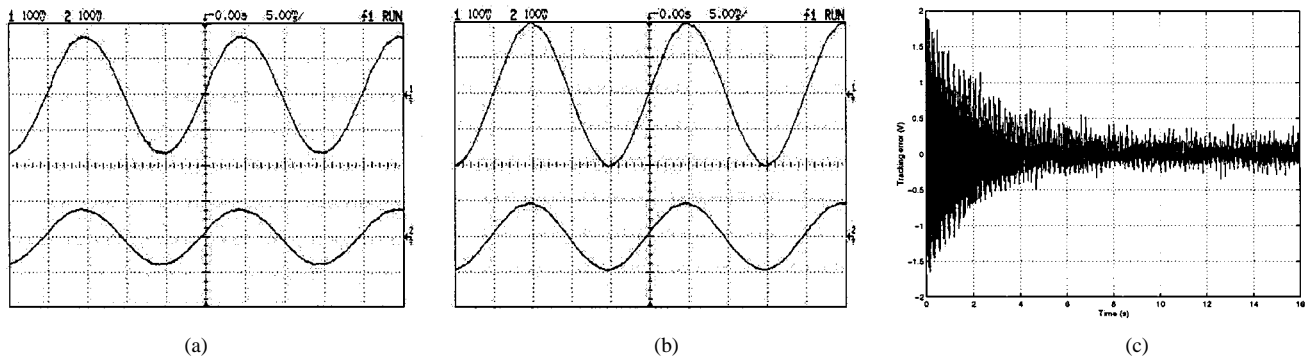
Fig. 9. Experimental results with resistance load.
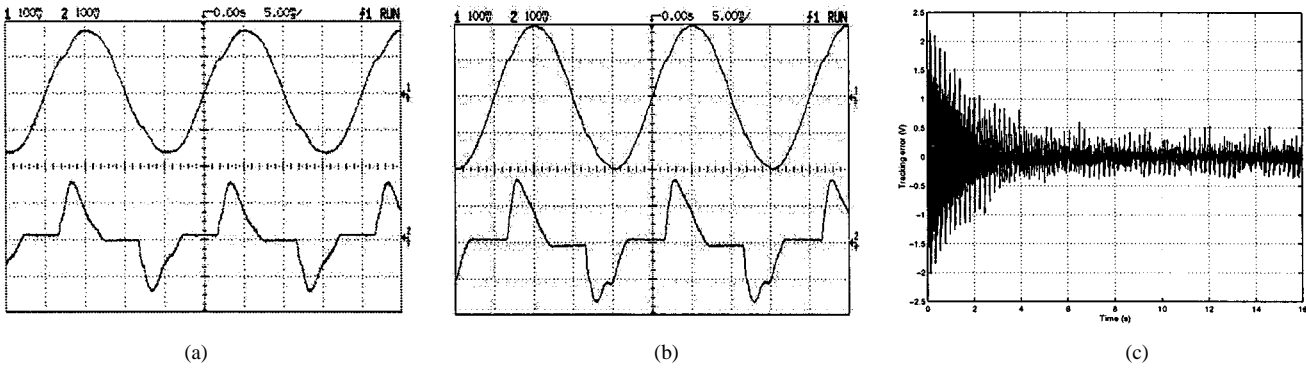
Fig. 10. Experimental results with uncontrolled rectifier load.

Output voltage is about 7.7 V with OSAP controller and is distorted by current surge with $\mathrm{THD} = 2\%$ as shown in Fig. 10(a); output voltage approaches 10 V and has less distortion $\mathrm{THD} = 0.7\%$ with OSAP plus repetitive controller in Fig. 10(b). Furthermore, Fig. 10(c) shows the peak of tracking error $e(t)$ is reduced from about 2.3 V to be less than 0.4 V after about 4 seconds when repetitive controller is plugged into the OSAP controlled converter. Nonideal effects, such as dead time for switches, computational time delay don't influence the experimental results in any significant way.

IV. EXAMPLE 2: THREE-PHASE BOOST-TYPE PWM RECTIFIER

The dynamics of the boost-type PWM rectifier (as shown in Fig. 11) can be described as follows [22], with the subscript $j = a, b, c$,

$$\dot{i}_j = -\frac{R_n}{L_n} i_j + \frac{1}{L_n}(E_j - v_j) \tag{26}$$

and

$$\dot{v}_d = -\frac{1}{C_n R_{\mathrm{on}}} v_d + \frac{1}{C} i_o + \frac{1}{C_n R_{\mathrm{on}}} E_L \tag{27}$$

where the neutral point M of dc bus is referred as the zero voltage point; phase currents i_a, i_b, i_c and dc bus voltage v_d are state variables; v_a, v_b, v_c are the PWM input voltages at port a, b, c; i_o is the PWM input current; E_a, E_b, E_c are the known 3-phase sinusoidal voltages and $E_a + E_b + E_c = 0$; L_n, C_n, R_n and R_{on} are the nominal values of the components; E_L is the *emf* of the load.

At the instantaneous basis, $v_j(t)$ $(j = a, b, c)$ and i_o can be written as

$$v_j(t) = \frac{1}{2} v_d(t) s_j \tag{28}$$

$$i_o = i_a s_a + i_b s_b + i_c s_c \tag{29}$$

where s_j $(j = a, b, c)$ are switching functions that are defined as: $s_j = +1$, when the switch S_{i+} is on and the switch S_{i-} is off; $s_j = -1$, when the switch S_{i-} is on and the switch S_{i+} is off. As shown in Fig. 11(b), each PWM switching waveform is a pulse of magnitude "+1" with width $t_{i+}(k)$ centered in the sampling interval T with its active duty ratio $d_j(k) = (t_{i+}(k) - (T - t_{i+}(k)))/(T) = (2t_{i+}(k))/(T) - 1$, where $-1 \leq d_j(k) \leq 1$, the subscript $j = a, b, c$.

The output equation is

$$y = [i_a \ i_b \ i_c \ v_d]^T. \tag{30}$$

The control objectives for the PWM rectifier system are to achieve: (1) unit power factor, i.e., the tracking phase errors between i_m $(m = a, b, c)$ and E_m $(m = a, b, c)$ approach zero asymptotically; (2) constant output dc voltage.

A. Controller Design

As shown in Fig. 12, a URZET control scheme of double-loop structure is proposed for the PWM rectifier: inner ac current-loop; outer dc voltage-loop [4].

1) URZET Current-Loop Controller: In sampled-data form, (26) can be approximately expressed as follows:

$$i_j(k+1) = \frac{b_1 - b_2}{b_1} i_j(k) + \frac{1}{b_1} E_j(k) - \frac{v_d(k)}{2} \frac{1}{b_1} u_j(k) \tag{31}$$

(a)   (b)
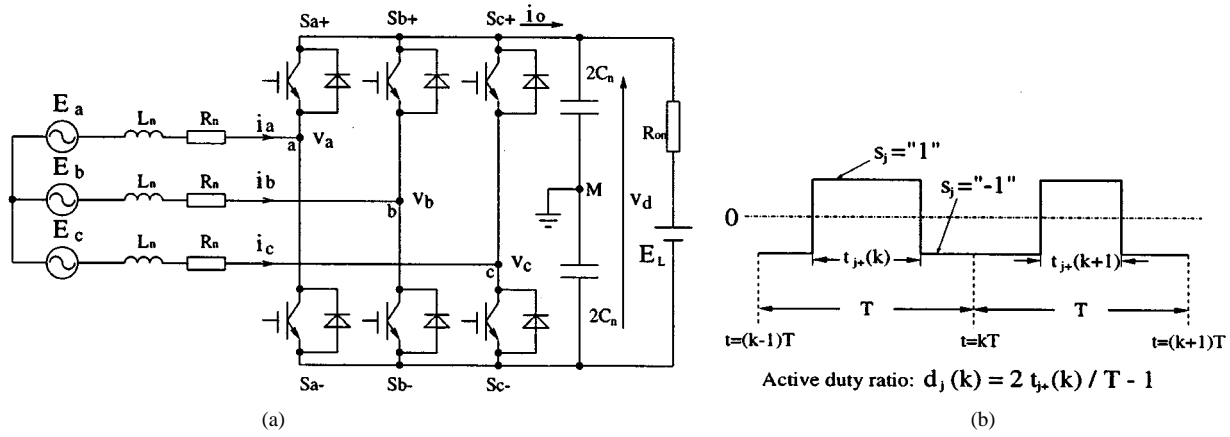
Fig. 11.   PWM rectifier and waveform of switching function.
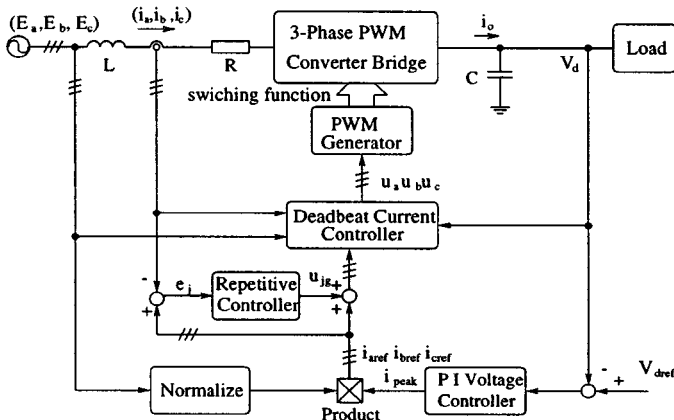
Fig. 12.   URZET controlled three-phase boost-type PWM rectifier.

where $u_j(k) = d_j(k)$; the subscript $j = a, b, c; b_1 = (L_n/T); b_2 = R_n; T$ is the sampling period.

It is clear that (31) can be treated as three independent current-loop subsystems. Conventional controller for each subsystem (31) can be chosen as follows:

$$u_j(k) = \frac{2}{v_d(k)}[E_j(k) - b_1 i_{j\,\text{ref}}(k) + (b_1 - b_2)i_j(k)] \quad (32)$$

(32) yields deadbeat response $i_j(k+1) = i_{j\,\text{ref}}(k)$ with transfer function $H(z) = z^{-1}$ for each subsystem. (32) is also referred to *predictive controller* in [3], [4].

Based on the URZET control theory in Section II, a URZET controller—repetitive current controller is proposed as follows to overcome the parameter uncertainties:

$$G_{gc}(z) = G_g(z)G_f(z) = \frac{k_g z^{-N+1}}{1 - z^{-N}} \quad (33)$$

where $G_f(z) = (1/H(z)) = z; G_g(z) = (k_g Q(z, z^{-1})z^{-N_1})/(1 - Q(z, z^{-1})z^{-N}); N_1 = N; N_2 = 0; Q(z, z^{-1}) = 1.$.

2) *Stability Analysis of Current Loop:* With consideration of parameter uncertainties ΔL and ΔR, the true transfer function $H_t(z)$ for the subsystem without repetitive controller (as shown in Fig. 13(a)) is

$$H_t(z) = \frac{b_1}{a_1 z - (a_1 - b_1) + (a_2 - b_2)} \quad (34)$$

where $L = L_n + \Delta L, R = R_n + \Delta R, a_1 = (L/T), a_2 = R$.

According to the stability analysis in Section II, the overall system is stable if both following conditions hold: (1) $\|((a_1 - b_1) - (a_2 - b_2)/a_1)\| < 1$; (2) $\|1 - k_g z H_t(z)\| < 1$.

3) *Voltage-Loop URZET Control–PI Control:* In the steady-state, from (29) and Fig. 12, we have $i_o = i_a s_a + i_b s_b + i_c s_c$ and $i_j \approx (E_j/\|E_j\|)i_{\text{peak}}$ (subscript $j = a, b, c$). Then $\|i_o\| \leq 3i_{\text{peak}}$ and the transfer function from i_{peak} to i_o can be approximately treated as

$$\frac{i_o(s)}{i_{\text{peak}}(s)} = \frac{k}{1 + \frac{T}{2}s} \quad (35)$$

where $-3 \leq k \leq 3$.

From (27), the transfer function from i_o to v_d can be obtained as

$$\frac{v_d(s)}{i_o(s)} = \frac{1}{Cs + 1/R_o}. \quad (36)$$

For dc signal $v_{d\,\text{ref}}$, discrete time PI controller is employed as follows:

$$G_v(z) = k_1 + k_2 \frac{T}{z - 1} \quad (37)$$

where k_1 and k_2 are designed to obtain a stable system with a satisfactory dynamic response.

The voltage-loop control subsystem is shown in Fig. 13(b). Proportional component in the PI controller is equivalent to the conventional controller $G_c(z)$ in Fig. 1; integral component in the PI controller is the plug-in URZET controller $G_{gc}(z)$ in Fig. 1. The stability of the closed voltage-loop control system can be analyzed through using *Routh—Hurwitz Criterion* in the frequency domain or the method mentioned in Section II in the z-domain.

B. Experiment

System parameter values are listed as follows.$L_n = 15$ mH; $L_1 = 19$ mH; $L_1 = 14$ mH; $L_1 = 19$ mH; $R_n = 0.5\ \Omega$; $R = 0.8\ \Omega$; $C_n = 5$ mF; $C = 0.47$ mF; $v_{d\,\text{ref}} = 80$ V; 3-phase sinusoidal voltages E_j ($j = a, b, c$) are 50 Hz 30 V (peak); $f_c = 1/T = 1.5$ kHz; $k_g = 0.02; N = 30; k_1 = 0.4; k_2 = 20; R_{on} = 100\ \Omega, E_L = 0$ V. Dead time for IGBT power switches is 3 μS. Computational time for the URZET control algorithm is about 70 μS.
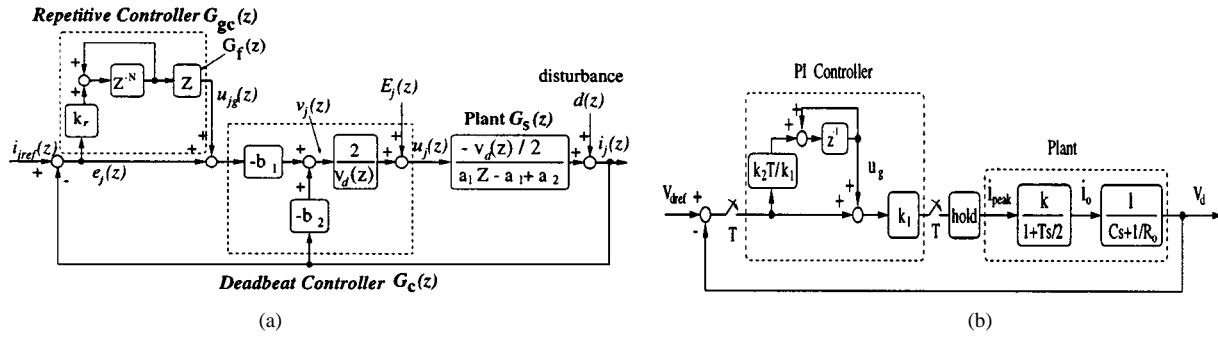
Fig. 13. URZET control of current-loop and voltage-loop.
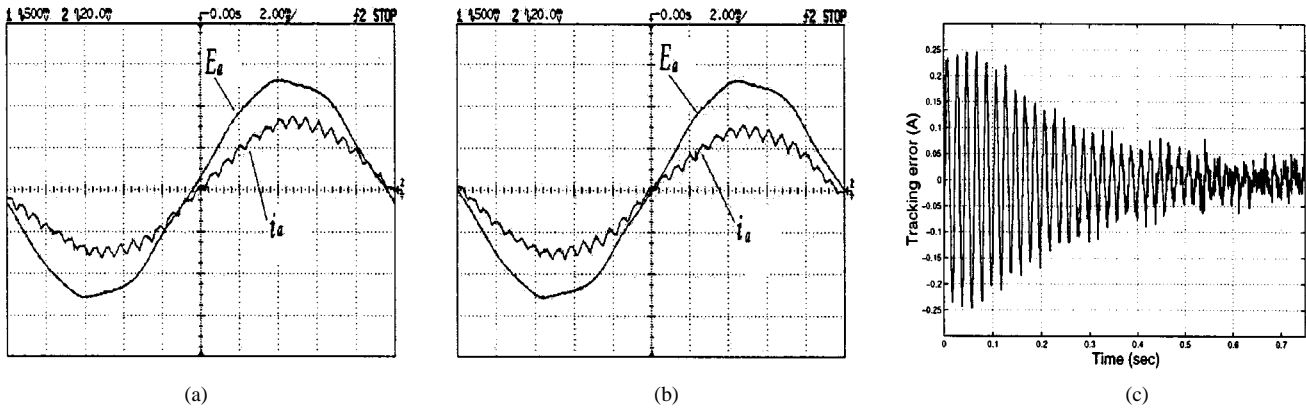
Fig. 14. Deadbeat and URZET controlled response.
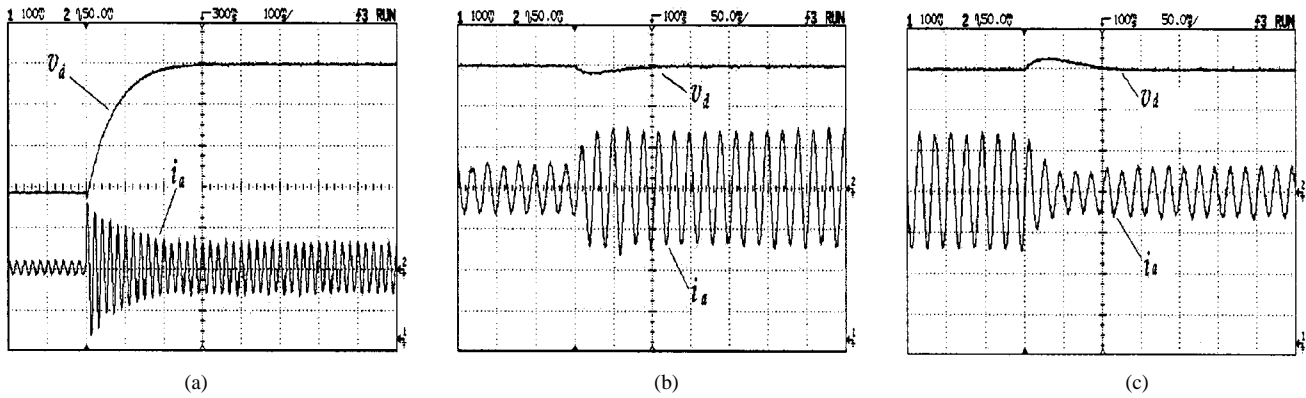
Fig. 15. PI controlled dc bus voltage $v_d(t)$ (12 V/div) and current $i_a(t)$ (2.5 A/div).

Fig. 14 shows a-phase steady-state current response of deadbeat controlled and URZET controlled PWM rectifier. In Fig. 14(a), from zero crossing points of both phase voltage $E_a(t)$ and phase current $i_a(t)$, we can see that there is a lag between $E_a(t)$ and $i_a(t)$. Fig. 14(b) shows that URZET controller force the phase displacement between $E_a(t)$ and $i_a(t)$ to approaches zero. Fig. 14(c) shows that the peak of current tracking error is reduced from 0.25 A to about 0.04 A after 0.7 s. Therefore, the power factor approaches unity. The response of other phase currents are similar to that of a-phase.

Fig. 15(a) and (b) and (c) show the PI controlled dc bus voltage response and current $i_a(t)$ response. In Fig. 15(a), $v_d(t)$ and $i_a(t)$ reach the expected value after about 0.3 sec in the start step response. Figure 15(b), (c) show that $v_d(t)$ returns to the reference value 80 V after about 0.1 sec under sudden load

disturbance. With PI controller, $v_d(t)$ can track the reference dc voltage with nearly zero error. Therefore, constant output dc voltage are achieved.

V. EXAMPLE 3: DC–DC PWM BUCK CONVERTER

The dynamics of the dc–dc PWM buck converter (as shown in Fig. 16(a)) can be described as follows [23]:

$$\begin{bmatrix} \dot{i}_L \\ \dot{v}_{\text{out}} \end{bmatrix} = \begin{bmatrix} 0 & -\dfrac{1}{L} \\ \dfrac{1}{C} & -\dfrac{1}{RC} \end{bmatrix} \begin{bmatrix} i_L \\ v_{\text{out}} \end{bmatrix} + \begin{bmatrix} \dfrac{1}{L} \\ 0 \end{bmatrix} v_{\text{in}} \quad (38)$$

where v_{out} is the output dc voltage; i_L is the inductor current; v_{dc} is the dc input voltage; L, C, and R are the values of the inductor, capacitor and load, respectively.
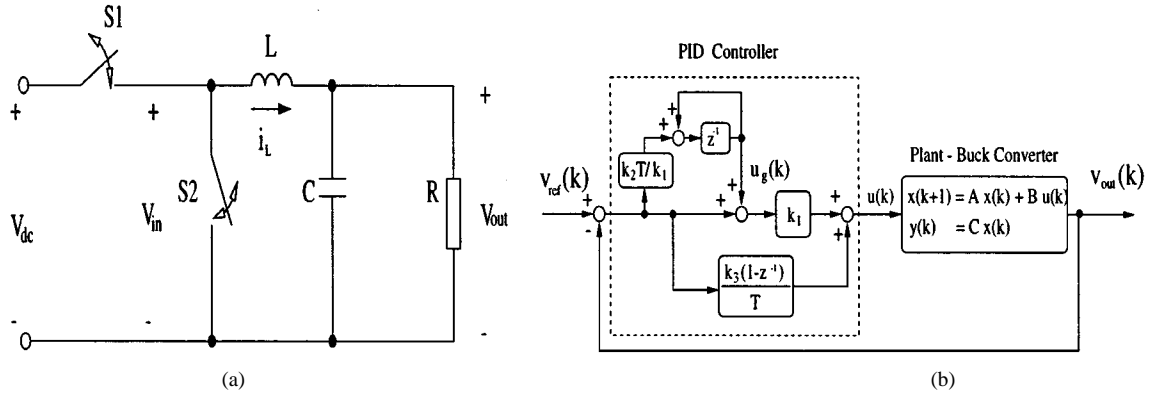
Fig. 16.   PWM buck converter and URZET control scheme.
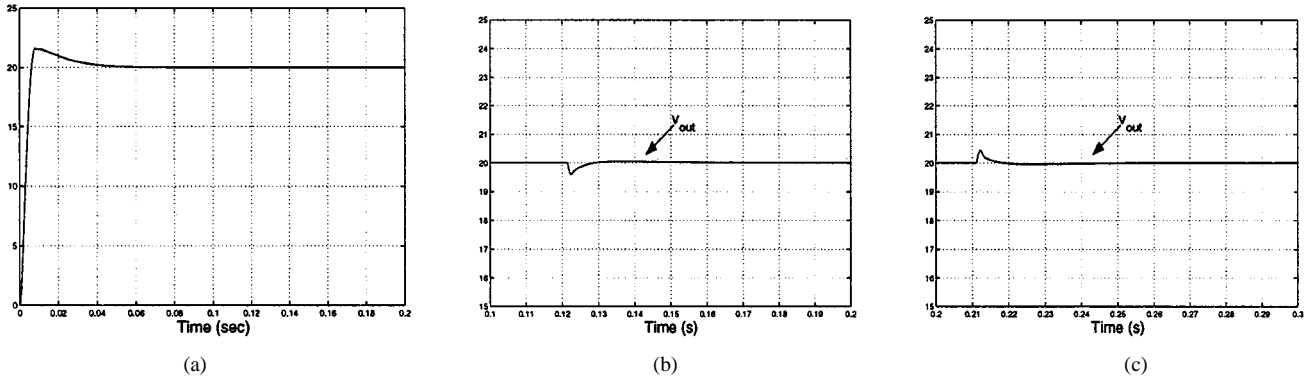
Fig. 17.   PID controlled output dc voltage v_{out}.

Neglecting the items of $o(T^2)$ or higher orders, sampled-data form for (38) can be written as follows:

$$\begin{bmatrix} i_L(k+1) \\ v_{\text{out}}(k+1) \end{bmatrix} = \begin{bmatrix} 1 & -\dfrac{T}{L} \\ \dfrac{T}{C} & 1 - \dfrac{T}{RC} \end{bmatrix} \begin{bmatrix} i_L(k) \\ v_{\text{out}}(k) \end{bmatrix} + \begin{bmatrix} \dfrac{1}{L} \\ 0 \end{bmatrix} u(k)$$

(39)

and its output equation is

$$y(k) = v_{\text{out}}(k) \tag{40}$$

where $u(k) = v_{\text{in}}(k) = v_{\text{dc}}\Delta T(k)$.

The control objective is to force v_{out} to track dc reference voltage v_{ref}.

A. URZET Voltage Control—PID Control

As shown in Fig. 16(b), PID controller tracking is chosen as follows:

$$u(k) = \left(k_1 + k_2 \frac{T}{z-1} + k_3 \frac{1-z^{-1}}{T} \right) (v_{\text{ref}}(k) - v_{\text{out}}(k)).$$

(41)

Based on the theory in Section II, in PID controller (41), PD component is referred to the conventional feedback controller $G_c(z)$; the integral component is the plug-in URZET controller G_{gc}. It can use the stability condition in Section II to determine the stable range of k_1, k_2 and k_3 for the PID controller. k_1, k_2, and k_3 are designed to achieve a stable system with a satisfactory dynamic response.

B. Simulation

Simulation parameters: $L = 4$ mH, $C = 6$ mF, $V_{\text{dc}} = 80$ V, $V_{\text{ref}} = 20$ V, $T = 4e^{-4}$ s, $k_1 = 0.25, k_2 = 15, k_3 = 1e^{-3}$.

The step response of output voltage is shown in Fig. 17(a). After about 60 ms, output voltage approaches reference value 20 V. Fig. 17(b) and (c) shows the output dc voltage response with load changes between ∞ Ω and 5 Ω. In both cases, $v_{\text{out}}(t)$ returns to the reference voltage $v_{\text{ref}} = 20$ V after about 0.03 second. With PID controller, $v_{\text{out}}(t)$ can quickly track the dc reference voltage with zero error. PID controlled dc-dc PWM buck converter maintains constant output dc voltage under load disturbances.

VI. DISCUSSION AND CONCLUSION

For ac reference input, the plug-in repetitive controller act as URZET controller for CVCF PWM converters. Comparing with feedback controllers, the size of the memory for the implementation of the repetitive controller is larger. If $Q(z, z^{-1}) = 1$, the size of the memory for the implementation of the repetitive controller $G_{gc}(z)$ is up to at least N units; if $Q(z, z^{-1}) = d_1 z + d_0 + d_1 z^{-1}$, the size of memory reaches at least $2N + 1$ units. Higher the sampling frequency f_c and the order of $Q(z, z^{-1})$ are, larger the size of memory is. Because the URZET controller adjusts its output once per period $T = 1/f$, it will take longer time to force the tracking error converge. However, feedback controllers have no memory and any imperfection in its performance of feedback control schemes will be repeated in all following cycles.

For dc reference input signal, integral controller is the URZET controller for CVCF PWM converters. PID controller is the proposed combined controller, where Proportional-Derivative or Proportional controller is the conventional feedback controller. Of course, other feedback control techniques such as the discrete sliding mode control with appropriate sliding surface may exhibits better dynamic performance in some cases of transient response. However, it is easier to design and implement PID control scheme.

The plug-in repetitive controller and the feedback controllers are complimentary: the fast dynamic response of the feedback controller and the high precision tracking ability of plug-in controller. Moreover, the dynamic response of our proposed URZETC scheme can be enhanced by adjusting the coefficients of the conventional feedback controller and the gain k_g of plug-in controller. Less the parameters uncertainties $(\Delta v, \Delta L, \Delta C, \Delta R)$ for the system are, less the residue tracking errors for conventional controller are. And the convergence rate of residue tracking error can be significantly accelerated by increasing the control gain k_g. What's more, repetitive learning control and iterative learning control have the advantageous capability to overcome nonmodelled dynamics [24], such as time delay. With dead-time for switches and computational delay for control algorithms etc., the experimental results show URZETC scheme is robust and effective.

The three examples of the URZET controlled CVCF PWM converters, such as CVCF PWM inverter, PWM rectifier and dc-dc PWM buck converter, show that the tracking errors caused by load disturbances, dc bus voltage derivation and parameter uncertainties can be eliminated by the proposed URZET controllers. The unified robust zero error tracking control of CVCF PWM converters provide a simple and efficient approach to the design of high-performance controllers for CVCF PWM converters. Simulation and experimental results demonstrate satisfactory performance of the proposed URZET controller.

REFERENCES

[1] A. Kawamura, T. Haneyoshi, and R. G. Hoft, "Deadbeat controlled PWM inverter with parameters estimation using only voltage sensor," *IEEE Trans. Power Electron.*, vol. 3, pp. 118–158, Mar. 1988.
[2] A. Kawamura, R. Chuarayapratip, and T. Haneyoshi, "Deadbeat control of PWM inverter with modified pulse patterns for uniterruptible power supply," *IEEE Trans. Ind. Electron.*, vol. 35, pp. 295–300, Apr. 1988.
[3] R. Wu, S. B. Dewan, and G. R. Slemon, "A PWM ac to dc converter with fixed switching frequency," *IEEE Trans. Ind. Applicat.*, vol. 26, pp. 880–885, Sept. 1990.
[4] ——, "Analysis of a PWM ac to dc voltage source converter under the predicted current control with a fixed switching frequency," *IEEE Trans. Ind. Applicat.*, vol. 27, pp. 756–764, Aug. 1991.
[5] M. Carpita and M. Marchesoni, "Experimental study of a power conditioning system using sliding mode control," *IEEE Trans. Power Electron.*, vol. 11, pp. 731–733, Sept. 1966.
[6] S. Muthu and J. M. S. Kim, "Discrete-time sliding mode control for output voltage regulation of three-phase voltage source inverters," in *Proc. IEEE Applied Power Electronics Conf. and Expo.*, 1998, pp. 129–135.
[7] H. Sira-Ramirez and M. Rios-Bolivar, "Sliding mode control of dc-to-dc power converters via extended linearization," *IEEE Trans. Circuits Syst. I*, vol. 41, pp. 652–661, Oct. 1994.
[8] A. Kawamura and R. G. Hoft, "Instantaneous feedback controlled PWM inverter with adaptive hysteresis," *IEEE Trans. Ind. Applicat.*, vol. 20, pp. 769–775, Aug. 1984.
[9] B. T. Ooi, J. C. Salmon, J. W. Dixon, and A. B. Kulkarni, "A 3-phase controlled current PWM converter with leading power factor," *Proc. IEEE IAS'85*, pp. 1008–1014, 1985.
[10] T. Haneyoshi, A. Kawamura, and R. G. Hoft, "Waveform compensation on PWM inverter with cyclic fluctuating loads," in *Proc. IEEE Power Electronics Specialist Conf.*, 1987, pp. 745–751.
[11] K. Zhou and D. Wang, "Digital repetitive learning controller for three-phase CVCF PWM inverter," *IEEE Trans. Ind. Electron.*, vol. 48, no. 4, pp. 820–830, 2001.
[12] ——, "Periodic errors elimination in CVCF PWM DC/AC converter systems: A repetitive control approach," *Proc. Inst. Elect. Eng. Controls Theory Applicat.*, vol. 147, no. 6, pp. 694–700, 2000.
[13] Y. Y. Tzou, S. L. Jung, and H. C. Yeh, "Adaptive repetitive control of PWM inverters for very low THD AC-voltage regulation with unknown loads," *IEEE Trans. Power Electron.*, vol. 14, pp. 973–981, Sept. 1999.
[14] S. L. Jung, H. S. Huang, and Y. Y. Tzou, "A three-phase PWM AC-DC converter with low switching frequency and high power factor using DSP-based repetitive control technique," in *Proc. IEEE PESC'98*, Fukuoka, Japan, May 1998, pp. 517–523.
[15] B. A. Francis and W. M. Wonham, "The internal model principle of control theory," *Automatica*, vol. 12, no. 5, pp. 457–465, 1976.
[16] M. Tomizuka, T. Tsao, and K. Chew, "Analysis and synthesis of discrete-time repetitive controllers," *Trans. ASME, J. Dyn. Syst. Meas. Control*, vol. 110, no. 3, pp. 271–280, 1988.
[17] M. Tomizuka, "Zero phase error tracking algorithm for digital control," *Trans. ASME, J. Dyn. Syst. Meas. Control*, vol. 109, no. 2, pp. 65–68, 1987.
[18] C. Cosner, G. Anwar, and M. Tomizuka, "Plug in repetitive control for industrial robotic manipulators," *Proc. IEEE Int. Conf. Robotics and Automation*, pp. 1970–1975, 1990.
[19] K. K. Chew and M. Tomizuka, "Digital control of repetitive errors in disk drive systems," in *Proc. American Control Conf.*, 1989, pp. 540–548.
[20] H. L. Broberg and R. G. Molyet, "Correction of period errors in a weather satellite servo using repetitive control," in *Proc. 1st IEEE Conf. on Control Application*, Dayton, OH, Sept. 1992, pp. 682–683.
[21] D. Wang, "On D-type and P-type ILC designs and anticipatory approach," *Int. J. Control*, vol. 73, no. 10, pp. 890–901, 2000.
[22] K. Zhou and D. Wang, "Zero tracking error controller for three-phase CVCF PWM inverter," *Electron. Lett.*, vol. 36, no. 10, pp. 864–865, 2000.
[23] D. M. Mitchell, *DC-DC Switching Regulator*. New York: Mc-Graw-Hill Company, 1988.
[24] M. Sun and D. Wang, "Initial condition issues on iterative learning control for nonlinear systems with time delay," *Int. J. Syst. Sci.*, to be published.

Keliang Zhou received the B.S. degree from Huazhong University of Science and Technology, Wuhan, China, and the M.S.E. degree from Wuhan University of Transportation, Wuhan, China, in 1992 and 1995, respectively. He is currently working toward the Ph.D. degree at Nanyang Technological University, Singapore.

His current research interests are in the fields of power electronics and electric machines, advanced control theory and applications.

Danwei Wang received the B. E. degree from the South China University of Technology, Guang Zhou, China, in 1982, and M.S.E. and Ph.D. degrees from the University of Michigan, Ann Arbor, in 1985 and 1989, respectively.

Since 1989, he has been with the School of Electrical and Electronic Engineering, Nanyang Technological University, Singapore, where he is currently an Associate Professor and Deputy Director of the Robotics Research Center. His research interests include robotics, control theory and applications. He publishes in the areas of manipulator/mobile robot dynamics, path planning, robust control, iterative learning control and adaptive control and their applications to industrial systems.